Journal of Engineering Mathematics **39:** 171–188, 2001.

On the asymptotic analysis of surface-stress-driven thin-layer flow

LEONARD W. SCHWARTZ
Department of Mechanical Engineering The University of Delaware Newark, Delaware 19716, U.S.A.

Received 5 January 2000; accepted in revised form 30 June 2000

Abstract. It has been demonstrated experimentally that thin liquid layers may be applied to a solid surface or substrate if a temperature gradient is applied which results in a surface tension gradient and surface traction. Two related problems are considered here by means of the long-wave or lubrication theory. In the first problem, an improved estimate of the applied liquid coating thickness for a liquid being drawn from a bath is found through asymptotic and numerical matching. Secondly, the theory is extended to consider substrates that are not perfectly wetted but exhibit a finite equilibrium contact angle for the coating liquid. This extension incorporates the substrate energetics using a disjoining pressure functional. Unsteady flows are calculated on a substrate of nonuniform wettability. The finite contact angle value required to stop stress-driven flow is predicted and the resulting steady profiles are compared with experimental results for several values of the applied stress.

Key words: thin-layer flow, asymptotic analysis, Marangoni effect, finite contact angle, numerical simulation.

1. Introduction

For most liquids the surface tension σ is a decreasing function of temperature. We consider a liquid layer that is bounded on one side by a solid surface, the substrate, and on the other side by a surface that is exposed to the atmosphere upon which surface tension acts. If the liquid layer is sufficiently thin, it is possible to assume that the temperature is virtually constant across the thin dimension. Then, if the substrate is nonuniformly heated, the temperature variation will be transferred to the free surface. The dimensionless criterion to be satisfied is that the Biot number, based on the liquid-film thickness, be very small [1]. The resulting temperature gradient on the free surface results in an applied shear stress given simply by

$$\tau = \sigma_x \ , \tag{1.1}$$

where x is measured along the substrate and subscripts are used to indicate differentiation [2].

The temperature-induced surface stress will contribute to the flow within the liquid layer. This is the well-known Marangoni effect. A number of basic theoretical studies have been performed in order to predict the resulting flow for thin liquid layers and isolated droplets on both flat and curved substrates [1, 3–5]. Recently interest has arisen in small devices that use this thermocapillary pumping mechanism to move microscopic quantities of liquid in medical and other applications [6].

Here we will be concerned with a liquid coating layer that is drawn from a bath onto a vertical plate using Marangoni stresses. Several experiments have been performed using a vertical plate that is partially submerged in a liquid bath [7–9]. A temperature gradient is applied to the plate in order to draw liquid upward. Two aspects of this problem will be considered here, as shown schematically in Figure 1. They are, (i) the prediction of the steady-state wetting-layer thickness that is drawn upward by use of a nominally-constant applied

shear stress, and (ii) the motion of the front of the rising liquid layer, particularly on a substrate of nonuniform surface energy, *i.e.* for a substrate where the equilibrium contact angle varies with position. In each of these two problems, within the approximation considered here, flow could also be driven by another source of applied surface stress such as a tangential wind stress. As indicated by the broken lines in the figure, the two regions considered are assumed to be separated by a long region over which the coating layer is flat, with thickness h_∞. Thus, for the steady-state problem (i), the layer of thickness h_∞ may be assumed to extend infinitely far upward.

A prediction of the layer thickness h_∞ that is drawn from the bath using the lubrication approximation was made by Fanton *et al.* [10]. The method is similar to the well-known prediction of the coating thickness that is deposited onto a vertical upwardly-moving plate, as treated by Landau and Levich (*viz.* Levich [11]). As in the Landau–Levich analysis, the leading-order prediction neglects the effect of gravity backflow. Compared with the experimental results of Cazabat *et al.* [8, 9] the predicted values of h_∞ in [10] are somewhat high. Here we will find the next term in the asymptotic expansion for layer thickness. The corrected prediction is closer to the experimental measurements. In addition, we solve the problem using a composite differential equation that is correct to the same order in the small parameter $\epsilon = \tau/\sqrt{\rho g \sigma}$. Here ρ is liquid density and g is the acceleration of gravity. The two different estimates are in substantial agreement when ϵ is small. The gravity correction for the stress-driven problem is shown to be of logarithmic order; it is thus a more important correction than the algebraic correction found by Wilson [12] for the Landau–Levich problem. Note that, although the fractional change in surface tension is small, the shear stress or surface tension gradient can be quite large. This is because changes in surface tension occur over quite short distances. Because the fraction change in surface tension is small, assigning a constant average value to σ in the capillary pressure term in each governing equation only introduces a small error.

While not discussed further in this paper, an interesting aspect of the experiments of Cazabat *et al.* [8, 9] is an observed transverse instability of the climbing front. This instability is associated with the appearance of a capillary ridge at the front. Linear stability analyses, performed by Kataoka and Trojan, provide an explanation for the instability [13, 14]. Recently we have modeled this unsteady three-dimensional motion and simulated the onset and nonlinear growth of the 'fingers' resulting from the instability [15]. Predicted finger shapes are in close agreement with the interferometric measurements given in [9].

In an earlier experiment, Ludviksson and Lightfoot [7] used a similar apparatus; however they considered smaller temperature gradients leading to thinner wetting layers. There was no tendency to form fingers; instead they were concerned with the speed and shape of the propagating front. Using observed values of the upstream thickness h_∞, and assuming the front to move at constant speed, Kataoka and Troian employed a lubrication model to get profile shapes similar to those observed experimentally [13, 14]. However, the observed values of h_∞ are significantly larger than those predicted by the bath withdrawal model and these large values remain largely unexplained. It should be noted that the withdrawal model predicts exceedingly small values, virtually of molecular dimensions for the squalane oil that was used. Carles and Cazabat [16] suggest that, since the experiment was performed with a plate that was initially partially submerged, insufficient time may have been taken to allow for complete drainage before the temperature gradient was applied.

In Section 3, we consider a second set of measurements made by Ludviksson and Lightfoot [7]. They applied a barrier coating of nonwetting material to the substrate. The front was found

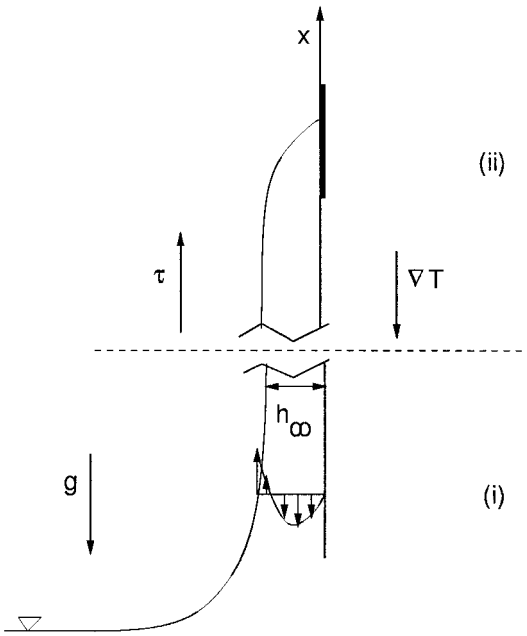

Figure 1. A liquid layer is drawn from a bath by a surface shear stress τ induced by a constant temperature gradient ∇T. The x-axis represents a solid vertical substrate. The darkened portion of the substrate signifies a region of larger equilibrium contact angle. Problem (i) is the prediction of the layer thickness h_∞ in bath withdrawal under steady-state conditions. Problem (ii) concerns the progression of the front tip onto a nonuniform substrate.

to stop at the barrier and the profiles were determined by means of interferometry for several values of the applied stress. We generalize the lubrication model to include the effect of finite equilibrium contact angle θ_e. A universal profile, in terms of dimensionless variables, is found for liquid fronts that come to rest against a barrier. These profiles are in reasonable agreement with the experimental results. We will find an analytic expression for the values of θ_e necessary to stop the frontal motion as a function of the physical parameters in the problem. These angles are remarkably small, much smaller than the contact angle for the strongly nonwetting coating that was applied in the experiment. Because patterns of coating are applied to control capillary-driven motions in real and contemplated microscopic devices, as discussed by Gau *et al.* [17] for example, predictions of barrier strengths are of importance.

Finite contact angle effects are added to the governing unsteady evolution equation through an additional interfacial effect known as disjoining pressure. Derived originally to quantify the magnitude of observed equilibrium contact angles in terms of molecular forces [18, 19], models incorporating disjoining effects can also be used in dynamic simulations that include frontal or contact-line motions on substrates that are not perfectly wetting [20–23]. Also included in Section 3 are dynamic simulations for motion up to and passing a barrier whose strength is insufficient to stop the flow. The general effect of such barrier passage is to increase the thickness of the coating layer. Recently unsteady simulations and analysis of thin-layer stress-driven motions, but without finite contact angle effects, have been reported by Bertozzi and co-workers [24–26].

2. The bath withdrawal problem

We wish to predict the thickness of the coating layer drawn from a bath using a given applied shear stress τ. This is problem (i) in Figure 1. The flow is assumed to be steady. If the x-axis is taken to point downwards, the constant flux Q in the drawn layer is given by

$$Q = \frac{\sigma h^3}{3\mu}\left[\frac{h_{xx}}{(1+h_x^2)^{3/2}}\right]_x - \frac{\tau h^2}{2\mu} + \frac{\rho g h^3}{3\mu} = -\frac{\tau h_\infty^2}{2\mu} + \frac{\rho g h_\infty^3}{3\mu}\,. \tag{2.1}$$

The idealized problem assumes that the drawn layer extends infinitely far upward, *i.e.* $x \to -\infty$, and the thickness is h_∞ there. The terms represent, respectively, the capillary pressure gradient driven flow, flow due to the upward stress and the downward gravity flow. The capillary pressure is proportional to the surface curvature $\kappa = h_{xx}/(1+h_x^2)^{3/2}$. Far upstream the curvature is zero and $h = h_\infty$. This equation employs the small-slope lubrication approximation and is equivalent to that used by previous workers [9, 13, 14]. We may derive this equation from the exact problem formulation by neglecting inertial effects and performing a systematic expansion in the free-surface slope, a so-called 'long wave' expansion, as demonstrated by Atherton and Homsy [27]. It can be seen from (2.1) that the value of the viscosity μ will not influence the shape of the steady-state profile.

Note that, to consistent order in the surface slope, the curvature gradient in (2.1) can simply be replaced by h_{xxx}. However, by retaining the full curvature, we observe that the equation includes the exact hydrostatic force balance $\sigma\kappa_x + \rho g = \text{const.}$ when $h \to \infty$. This limit corresponds to the static meniscus region where the tin layer meets the bath. The static meniscus represents the 'outer solution' to this problem. Equation (2.1) is thus a composite equation whose solution will give a complete approximation to the profile.

There are three length scales in this problem

$$L_* = \frac{2\sigma}{3\tau}, \quad L_c = \sqrt{\frac{\sigma}{\rho g}}, \quad h_\infty$$

and the scaling is $L_* \gg L_c \gg h_\infty$. Outer dimensionless variables are formed by use of the capillary length L_c,

$$h = L_c H, \quad x = L_c \xi\,,$$

and (2.1) may be rewritten as

$$\left[\frac{H_{\xi\xi}}{(1+H_\xi^2)^{3/2}}\right]_\xi = \epsilon\frac{H^2 - H_\infty^2}{H^3} - \left(1 - \frac{H_\infty^3}{H^3}\right)\,. \tag{2.2}$$

where

$$\epsilon = \frac{L_c}{L_*} = \frac{3}{2}\frac{\tau L_c}{\sigma} = \frac{3}{2}\frac{\tau}{\sqrt{\rho g \sigma}}\,. \tag{2.3}$$

For given constant values of ϵ, (2.2) may be integrated numerically by a 'shooting method' [28]. The shooting parameter is H_∞ whose values are found by a binary search until $H \to$ "∞" is satisfied. The integration is started on the thin layer. Fourth-order Runge–Kutta integration is used for this and other initial-value problems treated here.

For a slightly-perturbed coating layer, we linearize Equation (2.2) by assuming

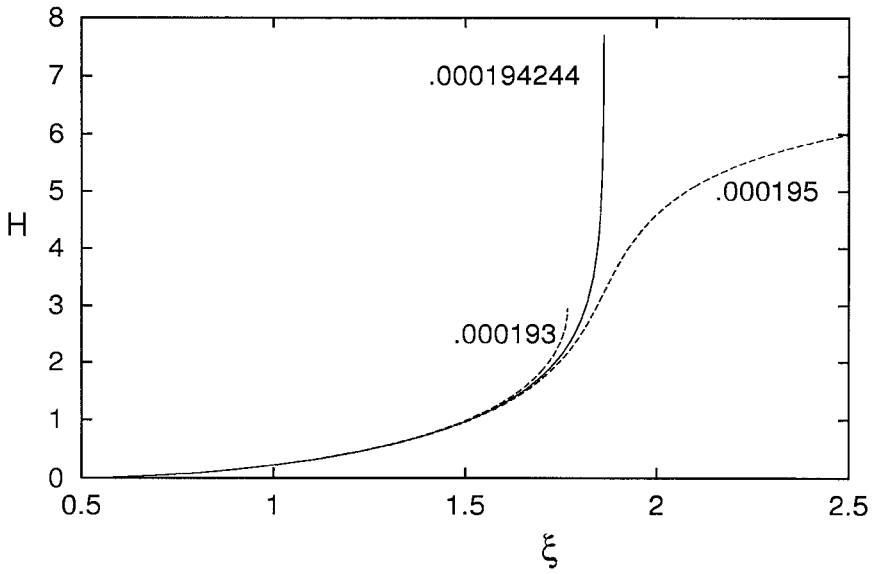

Figure 2. Dimensionless profile $H(\xi)$ determined by a shooting method for $\epsilon = 0{\cdot}01$. Numbers shown are values of the dimensionless wetting layer thickness H_∞. The accurate value is $H_\infty = 1{\cdot}942244 \times 10^{-4}$. Incorrect profiles are also shown for H_∞ values that are too small and too large.

$$H = H_\infty + g \ ,$$

where $g/H_\infty << 1$. The perturbation g satisfies

$$g_{\xi\xi\xi} = \left(\frac{2\epsilon}{H_\infty^2} - \frac{3}{H_\infty} \right) g \equiv Zg \tag{2.4}$$

with solution

$$g = \delta \exp(k\xi) \ , \tag{2.5}$$

where k is the positive real root of $k^3 = Z$. Equation (2.5) is used to generate initial conditions for the shooting solution, *i.e.*

$$H(0) = H_\infty + \delta, \quad H_\xi(0) = k\delta, \quad H_{\xi\xi}(0) = k^2\delta, \tag{2.6}$$

where $\delta \ll 1$. In practice δ is taken several orders of magnitude smaller than the shooting parameter H_∞. The criterion for success is simply $H \to \infty$ for some positive value of ξ, corresponding to the meniscus reaching the level of the bath. If H_∞ is too small, the slope H_ξ will become infinite at finite H, while for H_∞ too large, H will attain a maximum value and then decrease with increasing ξ.

A typical result of the shooting method is shown in Figure 2 for $\epsilon = 0{\cdot}01$. The figure shows the dimensionless profile $H(\xi)$ where the vertical plate corresponds to the ξ axis and the bath meniscus is on the right. The accurate value of the wetting layer thickness is $H_\infty = 1{\cdot}94244 \times 10^{-4}$ as indicated. Calculated profiles for larger and smaller H_∞ values are also shown. When H_∞ is too small, the profile achieves a horizontal tangent at a finite H value, while for overly large values, $H(\xi)$ reaches a maximum and then the profile turns back to the substrate. For a range of ϵ values, Table 1 compares the wetting-layer thicknesses found by the numerical shooting method with the results of the matching procedure to be discussed below.

Table 1. Dimensionless coating layer thickness H_∞ as a function of dimensionless shear stress ϵ.

ϵ	Numerical	2-term expansion (2.25)
10^{-5}	$2{\cdot}13518(10^{-10})$	$2{\cdot}13511(10^{-10})$
10^{-4}	$2{\cdot}13210(10^{-8})$	$2{\cdot}13167(10^{-8})$
10^{-3}	$2{\cdot}1078(10^{-6})$	$2{\cdot}1061(10^{-6})$
10^{-2}	$1{\cdot}9424(10^{-4})$	$1{\cdot}9389(10^{-4})$
0·1	$1{\cdot}2608(10^{-2})$	$1{\cdot}1521(10^{-2})$
0·3	0·0704	0·0534

C.f.: One term result: $H_\infty \approx 2{\cdot}135603\epsilon^2$.

The shooting solution of the composite equation will be compared with analytic approximations by the method of matched asymptotic expansions [29]. An equation valid within the thin layer will be integrated and matched to the capillary-static meniscus at the bath. Define inner variables according to

$$h = h_\infty \eta, \quad x = L\zeta \ ,$$

where

$$L = h_\infty^{2/3}\left(\frac{2\sigma}{3\tau}\right)^{1/3} = h_\infty^{2/3} L_*^{1/3} \ . \tag{2.7}$$

Equation (2.1) becomes

$$\left[\frac{\eta_{\zeta\zeta}}{\left(1+\left(\frac{h_\infty}{L_*}\right)^{2/3}\eta_\zeta^2\right)^{3/2}}\right]_\zeta = \frac{\eta^2-1}{\eta^3} - \hat{\epsilon}\left(1-\frac{1}{\eta^2}\right) \ . \tag{2.8}$$

with

$$\hat{\epsilon} \equiv \frac{2}{3}\frac{\rho g h_\infty}{\tau} = \frac{h_\infty}{L_c}\frac{L_*}{L_c} = \frac{H_\infty}{\epsilon} \ .$$

$\hat{\epsilon}$ will be shown to be $O(\epsilon)$ while H_∞ is $O(\epsilon^2)$.

The inner expansion is

$$\eta = \eta_0 + \hat{\epsilon}\eta_1 + \cdots \ , \tag{2.9a}$$

and the first two orders satisfy

$$\eta_{0\zeta\zeta\zeta} = \frac{\eta_0^2-1}{\eta_0^3} \ , \tag{2.9b}$$

and

$$\eta_{1\zeta\zeta\zeta} = \frac{3-\eta_0^2}{\eta_0^4}\eta_1 - 1 + \frac{1}{\eta_0^3} \ . \tag{2.9c}$$

Equation (2.9b) is analogous to the Landau–Levich equation for the prediction of the wetting layer on a drawn plate [11, 12] and is integrated in a similar way by the shooting method. Let $\eta = 1 + \phi$, $\phi \ll 1$, to obtain the linearized form

$$\phi_{\zeta\zeta\zeta} = 2\phi + O(\phi^2) \; . \tag{2.10}$$

The exponential growing solution of (2.10) gives the initial conditions

$$\eta_0(0) = 1 + \delta, \quad \eta_{0\zeta}(0) = 2^{1/3}\delta, \quad \eta_{0\zeta\zeta}(0) = 2^{2/3}\delta \; . \tag{2.11}$$

Unlike the Landau–Levich equation [11, 12]

$$\eta_{0\zeta\zeta\zeta} = \frac{\eta_0 - 1}{\eta_0^3} \; , \tag{2.12}$$

for which it is clear that $\eta_{0\zeta\zeta\zeta} \to 0$ as η_0^{-2} for η_0 large, for Equation (2.9b) the limiting values are approached more slowly. Accurate values can still be obtained, however, if we apply a straightforward refinement.

We seek the limiting value P_1 defined by

$$\eta_{0\zeta\zeta} \to P_1 \quad \text{as} \quad \zeta \to \infty \; .$$

Thus, η_0 approaches the parabola

$$\eta_0 \to P_1 \frac{\zeta^2}{2} \; .$$

Using (2.9b), we obtain a more accurate expression:

$$\eta_{0\zeta\zeta} \to P_1 + \int \frac{\mathrm{d}\zeta}{\eta_0} = P_1 + \int \frac{2}{P_1\zeta^2}\,\mathrm{d}\zeta = P_1 - \frac{2}{P_1\zeta} \; .$$

The corrected formula may be reverted to yield

$$P_1 = \left[\eta_{0\zeta\zeta} + \frac{2}{\zeta\,\eta_{0\zeta\zeta}}\right]_{\zeta\to\infty} + O\left(\frac{1}{\zeta^2}\right) \; , \tag{2.13}$$

which gives quadratic convergence, allowing equivalent accuracy to that obtainable for the moving-plate problem that uses (2.12). Marching the numerical solution gives a unique limiting value as $\zeta \to \infty$. It is found to be

$$\eta_{0\zeta\zeta} \to P_1 = 1{\cdot}8211895 \; . \tag{2.14}$$

The outer solution is the static meniscus satisfying

$$\left[\frac{H_{\xi\xi}}{(1 + H_\xi^2)^{3/2}}\right]_\xi = -1 \; .$$

whose shape is known in closed form. We use the profile $H(\xi)$ that has zero slope at $\xi = 0$. Princen [30] gives expressions for $H(\psi)$ and $\xi(\psi)$ where ψ is the positive downward inclination angle of the static profile with respect to the horizontal. These may be conbined to yield

$$H = H_0 + 0{\cdot}53284 - 2g - \frac{1}{2}\log\frac{1-g}{1+g} \tag{2.15a}$$

where

$$g = g(\xi) = \sqrt{1 - \frac{(\sqrt{2} - \xi)^2}{4}}\,, \tag{2.15b}$$

and $H = H_0$ at $\xi = 0$. H_0 is a matching constant to be determined.

From (2.15) we have $H_{\xi\xi}(0) = \sqrt{2}$ or $h_{xx}(0) = \sqrt{2}/L_c$. In a common set of variables this must be equal to the leading-order curvature found from the inner solution. Thus,

$$\eta_{0\zeta\zeta} = \frac{L^2}{h_\infty} h_{xx} = h_\infty^{1/3} \left(\frac{2\sigma}{3\tau}\right)^{2/3} h_{xx} \to h_\infty^{1/3} \left(\frac{2\sigma}{3\tau}\right)^{2/3} \frac{\sqrt{2}}{L_c}\,.$$

Solving this for h_∞ and using (2.14),

$$h_\infty = P_1^3 \left(\frac{3\tau}{2\sigma}\right)^2 \frac{L_c^3}{2^{3/2}} = \frac{9}{4} \left(\frac{P_1}{\sqrt{2}}\right)^3 \left(\frac{\sigma}{\rho g}\right)^{3/2} \left(\frac{\tau}{\sigma}\right)^2$$

or

$$H_\infty = \frac{h_\infty}{L_c} = \frac{P_1^3}{2^{3/2}} \epsilon^2 \approx 2{\cdot}135603\epsilon^2 = 4{\cdot}80511 \frac{\tau^2}{\rho g \sigma}\,. \tag{2.16}$$

This may be compared with the slightly larger result of Fanton *et al.* [10] which is $H_\infty = 4{\cdot}84\ \tau^2/(\rho g \sigma)$. The difference between our result and the earlier value is believed to be due to our use of the quadratically-convergent formula (2.13).

The next-order correction to (2.16) will now be found. The limiting equality

$$\eta_{0\zeta\zeta\zeta} \to \frac{2}{P_1 \zeta^2} \tag{2.17a}$$

can be integrated repeatedly to yield

$$\eta_0 \to \frac{P_1}{2}\zeta^2 - \frac{2}{P_1}\zeta \log \zeta + A\zeta + O(\log \zeta)^2\,. \tag{2.17b}$$

The next-order correction for the coating thickness is logarithmically dependent on ϵ and can be found analytically. For large ζ the equality (2.9c) is approximately

$$\eta_{1\zeta\zeta\zeta} = -1 - \frac{\eta_1}{\eta_0^2} + O\left(\frac{1}{\zeta^5}\right)\,. \tag{2.18}$$

Assume a solution of the form

$$\eta_1 = a_0 \zeta^3 + a_1 \zeta^2 \log \zeta + a_2 \zeta^2 + o(\zeta^2);$$

then

$$\eta_{1\zeta\zeta\zeta} = 6a_0 + \frac{2a_1}{\zeta}\,.$$

The right-hand side of (2.18) becomes

$$-1 - \frac{4a_0}{P_1^2 \zeta} + O\left(\frac{\log \zeta}{\zeta^2}\right)\,.$$

Thus

$$\eta_1 \to -\frac{\zeta^3}{6} + \frac{1}{3P_1^2}\zeta^2 \log\zeta + O(\zeta^2) \,.$$

and

$$\eta_{1\zeta\zeta} \to -\zeta + \frac{2}{3P_1^2}\log\zeta + \cdots \,.$$

Differentiaton of expansion (2.9a) now yields

$$\eta_{\zeta\zeta} = \eta_{0\zeta\zeta} + \hat{\epsilon}\eta_{1\zeta\zeta} + \cdots = P_1 - \hat{\epsilon}\zeta + \hat{\epsilon}\frac{2}{3P_1^2}\log\zeta + \cdots \,. \tag{2.19}$$

The origin of ζ must be shifted to match the outer solution. With

$$\zeta = \zeta_1 + \bar{\zeta} \tag{2.20}$$

we have

$$\eta_0 = \frac{P_1}{2}\bar{\zeta}^2 + \text{const.} = \frac{P_1}{2}(\zeta - \zeta_1)^2 + \text{const.} = \frac{P_1}{2}\zeta^2 - P_1\zeta_1\zeta + \text{const} \,.$$

Comparing with (2.17b), we find that

$$\zeta_1 = \frac{2}{P_1^2}\log\zeta - \frac{A}{P_1} \,. \tag{2.21}$$

Inserting (2.21) in (2.19), we get

$$\eta_{\bar{\zeta}\bar{\zeta}} = P_1 - \hat{\epsilon}\bar{\zeta} - \hat{\epsilon}\zeta_1 + \hat{\epsilon}\frac{2}{3P_1^2}\log\zeta + \cdots = P_1 - \hat{\epsilon}\bar{\zeta} - \hat{\epsilon}\frac{4}{3P_1^2}\log\zeta + O(\hat{\epsilon}) \,. \tag{2.22}$$

We return to outer variables with the transformations

$$\hat{\epsilon} = H_\infty/\epsilon, \quad \eta_{\bar{\zeta}\bar{\zeta}} = \frac{H_\infty^{1/3}}{\epsilon^{2/3}}H_{\xi\xi}, \quad \bar{\zeta} = \frac{\epsilon^{1/3}}{H_\infty^{2/3}}\xi \,.$$

Retaining the $O(\xi)$ term from the outer solution (2.15), we have

$$H_{\xi\xi} \to \sqrt{2} - \xi \quad \text{as} \quad \xi \to 0 \,.$$

Thus $\eta_{\bar{\zeta}\bar{\zeta}}$ may be equated to

$$\frac{H_\infty^{1/3}}{\epsilon^{2/3}}(\sqrt{2} - \xi) = P_1 - \frac{H_\infty}{\epsilon}\frac{\epsilon^{1/3}}{H_\infty^{2/3}}\xi - \frac{4}{3P_1^2}\frac{H_\infty}{\epsilon}\log\left(\frac{\epsilon^{1/3}}{H_\infty^{2/3}}\xi\right) + O(\epsilon) \,. \tag{2.23}$$

Let the corrected form of (2.23) be

$$H_\infty = \frac{P_1^3}{2^{3/2}}\epsilon^2(1 + \delta(\epsilon)) \,, \tag{2.24}$$

where

$$\delta = O(\epsilon\log\epsilon) \,.$$

Inserting this expression in (2.23) and expanding for small δ, we obtain

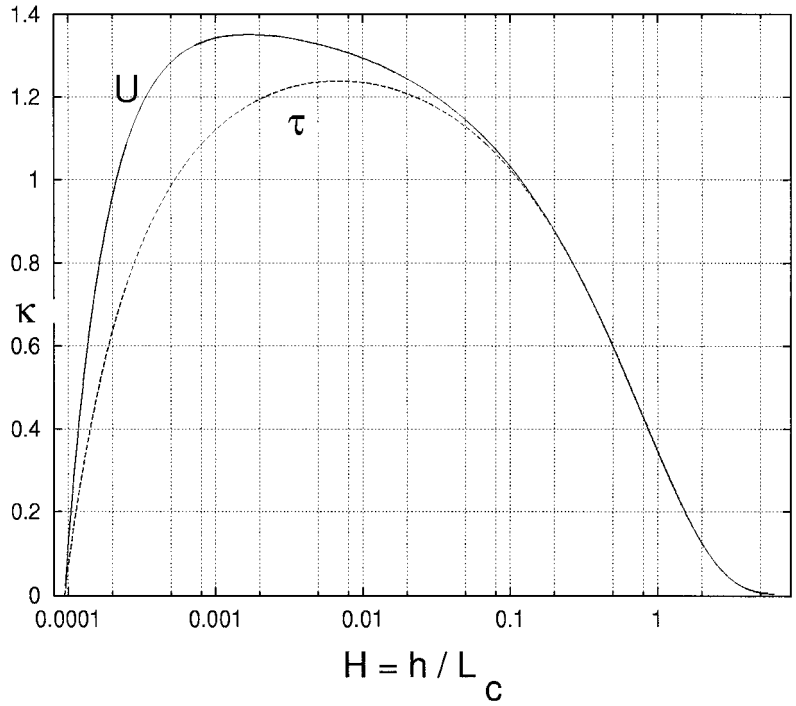

Figure 3. Numerical solutions for the dimensionless curvature κ versus distance from the wall $H = h/L_c$ for the Landau–Levich plate drawing problem, labelled U, and stress-driven problem, labelled τ.

$$P_1(1+\delta)^{1/3} \approx P_1\left(1+\frac{1}{3}\delta\right) = P_1 - \frac{\sqrt{2}}{3}P_1\epsilon\log\left(\frac{2\epsilon^{1/3}}{P_1^2\epsilon^{4/3}}\xi\right) .$$

As $\epsilon \to 0$, this becomes simply

$$\delta = \sqrt{2}\epsilon\log\epsilon + O(\epsilon) .$$

From (2.24) the corrected expression for H_∞ is

$$H_\infty = 2{\cdot}135603\epsilon^2 + 3{\cdot}020199\epsilon^3\log\epsilon + O(\epsilon^3) . \tag{2.25}$$

Values calculated using (2.25) for various ϵ are shown in Table 1 where they may be compared with the shooting-method results.

Compared with the leading-order result, Equation (2.25) provides sowewhat closer agreement with the experimental measurement of Fanton *et al.* [10]. From the experimental values $\tau = 0{\cdot}9$ dynes/cm^2, $\sigma = 21$ dynes/cm, and $\rho = 0{\cdot}965$ gm/cm^3 we have the value $\epsilon = 0{\cdot}00960$. Using this ϵ, we observe that the leading-order theory predicts $h_\infty = 0{\cdot}293$ μm, while both the two-term expansion and the shooting-method give $0{\cdot}266$ μm. The experimentally measured thickness was $0{\cdot}23 \pm 0{\cdot}06$ μm, where the error brackets come from measurement uncertainty. While still too large, the more accurate prediction lies well within the bracketed uncertainty.

It is interesting to compare the profiles $h(x)$ for stress-driven motion as considered here with those obtained for the Landau–Levich plate withdrawal problem [11]. A composite equation for plate withdrawal, analogous to (2.2), is

$$\left[\frac{H_{\xi\xi}}{(1+H_\xi^2)^{3/2}}\right]_\xi = 3\mathrm{Ca}\frac{H-H_\infty}{H^3} - \left(1-\frac{H_\infty^3}{H^3}\right) . \tag{2.26}$$

where $\mathrm{Ca} = \mu U/\sigma$ and U is the constant plate withdrawal speed. Initial conditions for this composite equation are derived from

$$g_{\xi\xi\xi} = \left(\frac{3\mathrm{Ca}}{H_\infty^3} - \frac{3}{H_\infty}\right) g$$

which is analogous to (2.4). Two profiles are compared in Figure 3 where the dimensionless curvature $\kappa = H_{\xi\xi}/(1+H_\xi^2)^{3/2}$ is plotted versus H. A logarithmic scale is invoked to magnify the wall region. The curve labeled U is the plate-withdrawal solution, while τ indicates the stress-driven case. Values of ϵ and Ca are selected so that $h_\infty/L_c \approx 10^{-4}$ for each case. Note that the region in which dynamic effects are important is much larger for the shear-driven problem. In these cases the profile joins the static meniscus at a far greater distance from the wall.

3. Thin-layer motion on nonuniform substrates

In the earlier experiment of Ludviksson and Lightfoot [7] a coating of nonwetting material was applied to the substrate in order to control the motion of the liquid. Here we will generalize the lubrication model to include finite-contact-angle effects. We will be concerned with the unsteady motion of a thin layer whose thickness is constant far upstream; specifically we consider problem (ii) shown in Figure 1. The slope of the free surface relative to the substrate will be assumed to be uniformly small, so that the lubrication approximation can continue to be used.

Problem (ii) involves the motion of a three-phase contact line, *i.e.* a line where the solid substrate, the advancing liquid, and vapor or vacuum meet. It is well known that such a problem requires special treatment. Unless the no-slip boundary condition for the liquid motion on the solid substrate is relaxed in the vicinity of the contact line in some way, one obtains the anomalous result that infinite force is required to move the contact line [31]. A number of modifications that allow motion of the contact line were compared by Moriarty and Schwartz [32]. They found that, apart from the immediate vicinity of the contact line, each choice of relief mechanism yielded the same set of moving liquid profiles. The simplest modification is to 'pre-wet' the substrate ahead of the moving contact line with a very thin layer of the liquid, *i.e.* a slip layer [28]. In addition, for liquids that do not spread spontaneously onto the substrate, a static or equilibrium contact angle θ_e is observed. By appending a disjoining pressure term to the usual capillary pressure, it is possible to prescribe both the thickness of the slip layer and the contact angle θ_e, as explained below.

Returning to the lubrication approximation in dimensional variables, with upward surface traction and downward gravity flow, we observe that the flux is given by

$$Q = -\frac{h^3}{3\mu} p_x + \frac{\tau h^2}{2\mu} - \frac{\rho g h^3}{3\mu} \,. \tag{3.1}$$

The pressure p is composed of the usual capillary pressure associated with free-surface curvature and a disjoining pressure component that can be used to specify an equilibrium contact angle θ_e. θ_e will be taken to vary with position on the substrate. Thus

$$p = -\sigma h_{xx} - \Pi \,, \tag{3.2}$$

where we will use

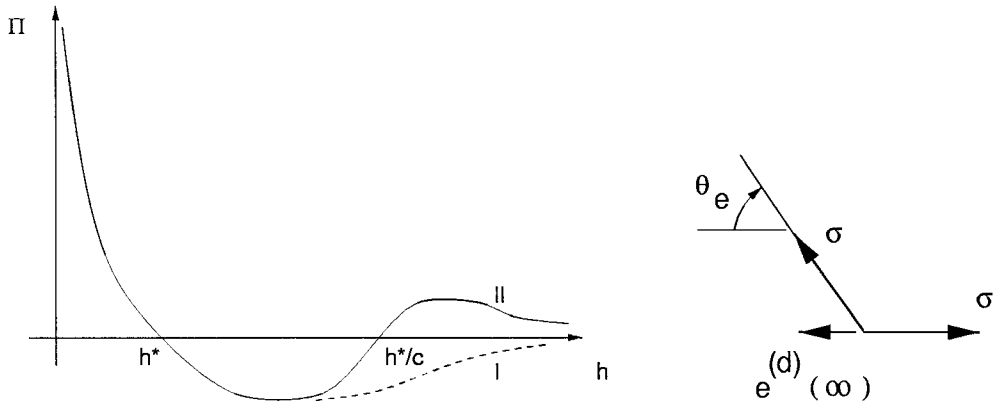

Figure 4. Left: Two different forms of the disjoining pressure function Π plotted versus liquid layer thickness h. *Right*: The contact-line force balance using disjoining pressure. θ_e is the static or equilibrium contact angle.

$$\Pi = K\left(\frac{h^*}{h}\right)^2\left(\frac{h^*}{h}-1\right)\left(\frac{h^*}{h}-c\right)\ . \tag{3.3}$$

This function represents an assumed interaction between the substrate and the liquid free surface. The constant h^* plays the role of a slip coefficient, while K will be shown to incorporate information about the equilibrium angle θ_e.

The form of Π used here is only one of a number of possible choices, since the full details of the molecular interactions in real systems are not known. Different exponents on h could have been used, for example. The formula (3.3) does include the two basic behaviors that allow for a finite value of θ_e to be specified. Typically schematic plots of $\Pi(h)$ are shown in Figure 4. If the constant c is taken to be zero, $\Pi < 0$ for $h > h^*$. In that case, layers thicker than h_* will be attracted downward. That is the case indicated by (I) in the figure. Alternatively, as indicated by (II), if $c > 0$, sufficiently thick layers will be stable and the disjoining pressure will become repulsive for $h > h^*/c$. Each of these forms is possible and the particular choice depends on the specific liquid-substrate material system, as discussed by Teletzke *et al.* [20] and Churaev and Sobolev [18]. We have performed dynamic simulations in related problems with various exponent choices and find that appreciable differences in profile shape only occur in the immediate neighborhood of the apparent contact line, while the larger scale dynamics is virtually the same [22, 23].

Associated with Π is a disjoining energy density

$$e^{(d)}(h) = -\int_{h^*}^{h}\Pi(h_1)\,\mathrm{d}h_1\ . \tag{3.4}$$

which represents the work done against disjoining pressure in displacing an element of the liquid-air interface from its equilibrium value $h = h^*$. Consider a wedge of liquid that meets the apparent substrate and whose ultimate thickness is large when measured in units of h^*; *i.e.* we consider $h/h^* \to \infty$. Integration of (3.4) yields

$$e^{(d)}(\infty) = Kh^*\left(\frac{1}{6}-\frac{c}{2}\right)\ . \tag{3.5}$$

The right side of Figure 4 shows the static force balance at the effective 'contact line,' where a thick layer meets the slip layer $h = h^*$. From the figure, when θ_e is small,

$$e^{(d)}(\infty) = \sigma(1 - \cos\theta_e) \approx \frac{\sigma\theta_e^2}{2} \,. \tag{3.6}$$

Equating the two expressions for $e^{(d)}(\infty)$, we obtain an explicit expression for K in terms of the contact angle

$$K = \frac{3\sigma\theta_e^2}{h^*(1-3c)} \,,$$

indicating that the meaningful range for c is $0 \leq c < 1/3$. When Π is inserted in the evolution equation, it provides a method for modeling motion on substrates that exhibit a finite static contact angle. Moreover, it will illustrate the way in which lack of perfect wetting influences motion. Disjoining pressure was introduced in order to explain the molecular origins of static contact angles. For particular material systems, some progress can be made in calculating the exponents and constants that appear in an expression such as (3.3) from first principles [33]. The important features of (3.3), in a dynamic study, are the values of θ_e and h^* and the fact that there is a single stable minimum of the energy functional $e^{(d)}(h; h^*)$.

Ludviksson and Lightfoot [7] include results of a series of experiments where a barrier of non-wetting coating was applied to the substrate. As expected, the wetting front stopped at this barrier. We will consider these results as a special case of unsteady motions on substrates with barriers.

With motion in the direction of x increasing, we may form an unsteady evolution equation using the integral mass conservation condition

$$h_t = -Q_x \tag{3.7}$$

where Q is given by (3.1) and (3.2). A number of parameters can be removed by the scaling

$$t = T^*\tilde{t}, \quad x = L\tilde{x}, \quad h = h_0\tilde{h} \,, \tag{3.8}$$

where $h_0 = 3\tau/(2\rho g)$, $L = h_0^{1/3}L_c^{2/3}$, $T^* = 3\mu L^4/(\sigma h_0^3)$, and, as before, $L_c = \sqrt{\sigma/(\rho g)}$. The dimensionless evolution equation with tildes omitted is

$$h_t = -\left[h^3 h_{xxx} + h^2 - h^3\right]_x - \left[h^3\left(D\tilde{\Pi}\right)_x\right]_x \,. \tag{3.9}$$

Here

$$\tilde{\Pi} = \left(\frac{h^*}{h}\right)\left(\frac{h^*}{h} - 1\right)\left(\frac{h^*}{h} - c\right) \,. \tag{3.10}$$

Dimensionless variables are used on the right of (3.10) and

$$D = 3\left(\frac{L_c}{h^*}\right)\left(\frac{L_c}{h_0}\right)^{1/3}\frac{\theta_e^2}{1-3c} \,. \tag{3.11}$$

For a steady solution in laboratory-fixed coordinates we have $Q = 0$; then, in dimensionless terms, $h = 1$ is the layer thickness far upstream where $p_x = 0$. Since disjoining effects are only important when $h \sim O(h^*)$ and $h^* << 1$, a universal steady-state differential equation,

$$h_{xxx} = \frac{h-1}{h} \,, \tag{3.12}$$

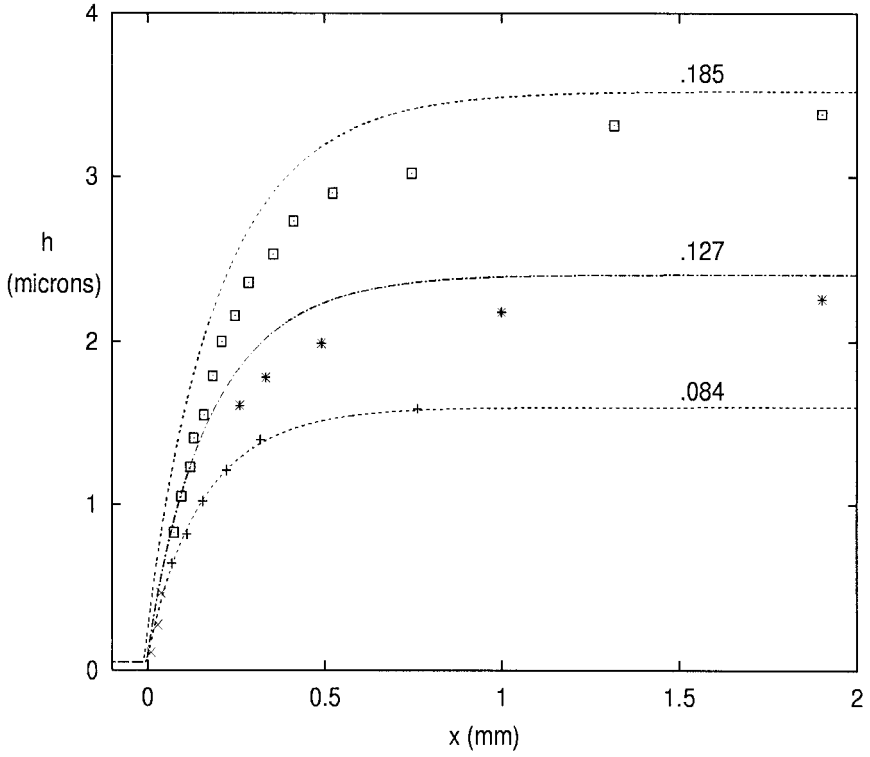

Figure 5. Comparison of calculated steady profiles at a barrier with experimental data of Ludviksson and Lightfoot [7] (symbols). The shear stress values, taken from the experiment results, are $\tau = 0{\cdot}084$, $0{\cdot}127$, and $0{\cdot}185$ dynes/cm^2.

determines the steady profile away from the apparent contact line. There is an essentially unique solution of (3.12) that meets the substrate. The initial conditions are found from the upstream approximate solution

$$h \approx 1 - \delta \exp(kx) \,, \tag{3.13}$$

where δ is a small positive number. The linearized form of (3.12) shows that $k = 1$. Runge-Kutta integration of (3.12) yields the universal static profile. This effective outer solution has finite contact slope K_s at $h = 0$. If the profile is translated so that the contact point corresponds to $x = 0$, a local solution there is

$$h \sim K_s \hat{x} + \frac{\hat{x}^2}{2K_s} \log \hat{x} + O(\hat{x}^2) \,, \tag{3.14}$$

where $\hat{x} = -x$ is used here. From the initial condition (3.13), the universal value

$$K_s = 1{\cdot}34544 \ldots \tag{3.15}$$

is found by integration.

Ultimate profiles at a barrier may be calculated from the evolution equation (3.9) with rather general initial conditions. The equation is written in finite-difference form. An implicit time-marching algorithm has been implemented leading to greatly improved numerical stability and the ability to use much larger time steps. Generally speaking, the method is a

higher-order generalization of the Crank–Nicolson method that is commonly used to solve the heat equation. Additional details of the numerical method may be found elsewhere [34, 35]. The contact angle variation $\theta_e(x)$ is prescribed and is taken to rise rapidly from zero to a finite value in a particular region of the substrate. When the moving front reaches the barrier region it stops and, after a period of adjustment to the upstream thickness, the entire profile becomes steady. Calculated profiles are compared with the experimental results of Ludviksson and Lightfoot in Figure 5. Three different values of imposed shear stress are shown; each is derived from the measured temperature gradient and the measured dependence of surface tension on temperature. The agreement is credible but not perfect. Better agreement is observed for the smallest τ value. The three data points marked by (x) are said to be applicable to all profiles. Thus, Ludviksson and Lightfoot [7] maintain that the contact angle is independent of τ; this differs from the result of the present analysis. We can predict the actual contact angle θ_e^* required to arrest the stress-driven motion, using the value for K_s and returning to dimensional quantities via (3.8):

$$\theta_e^* \approx K_s \frac{h_0}{L} = 1{\cdot}762 \left(\frac{\tau}{\sqrt{\sigma \rho g}} \right)^{2/3} . \tag{3.16}$$

For $\tau = 0{\cdot}185$ dynes/cm^2, which is the largest shear stress applied in the barrier experiments of Ludviksson and Lightfoot, the predicted contact angle required to stop the motion is $\theta_e^* \approx 1{\cdot}1$ degrees. Thus, the strongly nonwetting coating that they applied was far stronger than needed to arrest the motion of the contact line.

Figure 5 shows that unsteady solutions each approach the universal steady state if the barrier 'height', meaning the maximum equilibrium contact angle, is sufficiently high. The specific value of maximum contact angle used in the numerical solution of (3.9) was $1{\cdot}2°$. The slip layer thickness h^* was taken to be 50 nanometers, an arbitrarily chosen but realistically small value. In Figure 5 the direction of motion is from right to left. This is the direction used in the original plot of the experimental data given in [7].

Two of the three final profiles from Figure 5 are replotted in Figure 6 in dimensionless variables. The universal solution from (3.12) is also shown as a line. The symbols use the extreme values of shear stress in the experiments, $\tau = 0{\cdot}084$ dynes/cm^2 and $0{\cdot}185$ dynes/cm^2, respectively. The layer thickness h is measured in units of $3\tau/(2\rho g)$ so that the limiting height far away from the barrier is one. In these units, the dimensionless slip layer thickness depends on τ, as shown in the figure. Because the barrier is quite steep, *i.e.* the contact angle changes from zero to $1{\cdot}2°$ over a short distance on the substrate, the unsteady profiles stabilize in almost the same position. The origin of the universal solution is arbitrary. It was shifted so as to illustrate the self similarity of the steady profiles.

Results of another unsteady calculation are shown in Figure 7. Here the barrier 'height' was taken to be smaller than the value required to stop the motion; specifically the contact angle $\theta_{e\,\max}$ is 60 per cent of the critical value of θ_e^*; given by (3.16). The dimensionless slip-layer thickness is $h^* = 0{\cdot}02$. The calculation used 2500 unknown values of h and a point-spacing interval $\Delta x = 0{\cdot}025$.

The direction of motion is from left to right and values of the dimensionless time are shown on each profile. To the left of the barrier $\theta_e = 0$. An initial profile was arbitrarily chosen to be an inverse tangent curve connecting the uniform upstream thickness and the slip layer. The argument of the inverse tangent is scaled so that 70 per cent of the jump in h occurs in $0{\cdot}2$ x units. Similarly, the contact-angle function $\theta_e(x)$ is also an arc tangent whose argument is scaled so that 70 per cent of the jump occurs in $1{\cdot}0$ x units. The profile is seen to quickly

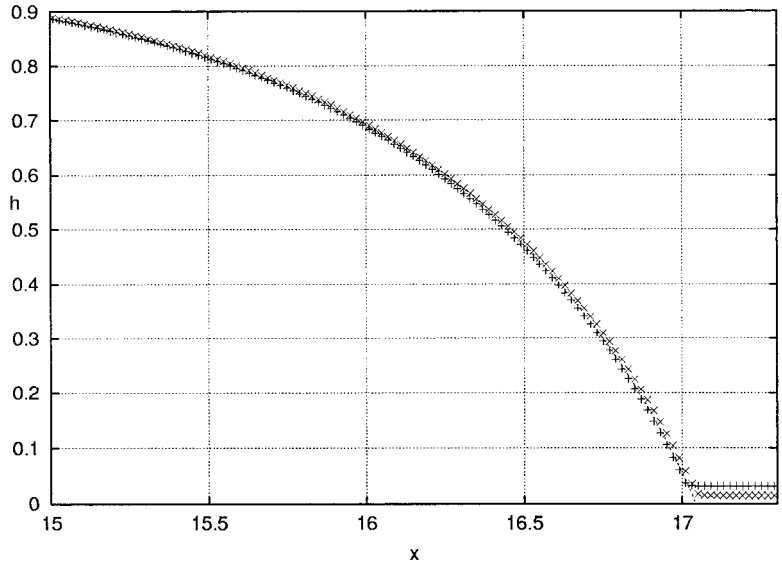

Figure 6. Unsteady calculations are compared with the universal outer solution (line) using dimensionless variables. Each unsteady solution using the same physical slip layer $h^* = 50$ nm. The symbols correspond to the two extreme experimental values of shear stress $\tau = 0{\cdot}084$ dynes/cm^2 and $0{\cdot}185$ dynes/cm^2.

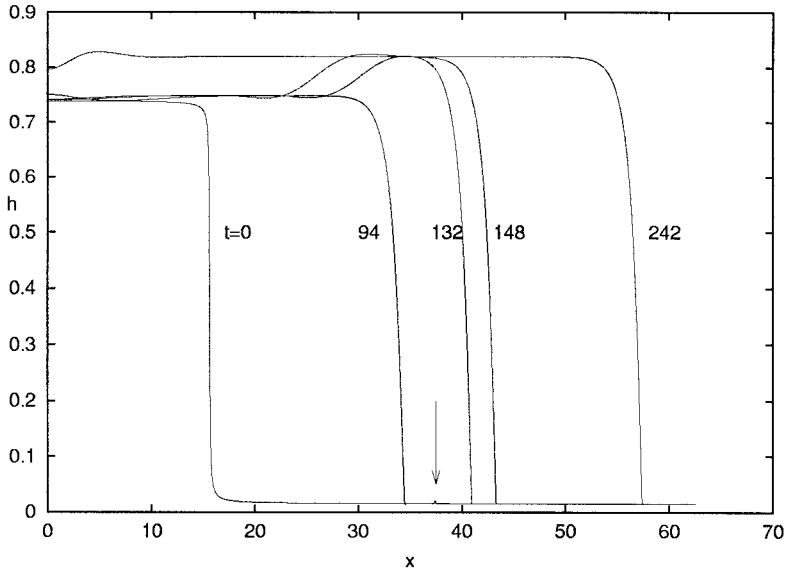

Figure 7. Unsteady calculation of a moving front involving the evolution equation (3.9). The equilibrium contact angle θ_e is a function of substrate position and 'ramps up' from zero, on the left of the arrow to a finite value on the right. The final value of θ_e is too small to stop the motion. Dimensionless time values are shown for each profile.

reform into a unique steadily-propagating shape that is determined by the upstream height and h^*. Upon reaching the location of the barrier, indicated by an arrow in the figure, the profile temporarily slows and forms a hump. Ultimately the upstream height is adjusted upward. This is a simple illustration of the manner in which substrate contact-angle variation may be used to adjust the shape of a flowing stream. The calculation of Figure 7 was repeated using the second form of disjoining pressure with $c = 0{\cdot}1$, as indicated by (II) in Figure 4. Quite similar

results were obtained; the major difference was that final height after barrier passage was slightly higher.

Concluding remarks

Two aspects of shear-stress driven flow have been considered. Estimates of coating thicknesses produced under steady-state conditions of bath withdrawal have been refined using two different methods. Each of these account for the gravitational backflow into the bath. Provided that the shear stress is not large, they are in substantial agreement with one another and provide an improved agreement with the experimental result of Fanton *et al.* [10]. The asymptotic expansion has been extended to include a term of order $\epsilon^3 \log \epsilon$. This term is missing from the expansion for the related Landau-Levich problem of plate withdrawal where the correction term is of order ϵ^3, as found by Wilson [12]. The wall region, where viscous effects are important, is thicker for the stress problem. We believe that extension of the solution to order ϵ^3 for the stress case may require a third or intermediate, matching region [29].

An unsteady evolution equation has been introduced to model motion on a substrate of non-zero and variable contact angle. The critical value of contact angle θ_e^* required to stop the motion has been found and is predicted to be proportional to the two-thirds power of applied shear stress. The actual values of θ_e^* are remarkably small, far smaller than that of the 'strongly nonwetting' coating applied by Ludviksson and Lightfoot [7] to arrest the motion. Our results concerning the behavior θ_e^* differ qualitatively from a conjecture given in [7]. Those authors had suggested that there is a universal value of θ_e^*, for a particular liquid-solid system, that is independent of the driving stress τ. For smaller contact angle changes, it has been shown that the shape of the moving liquid stream can be modified and controlled by the pre-set variation in contact angle. Possible applications include thermocapillary pumping devices and other microscopic liquid transport mechanisms.

Acknowledgement

This work is supported by the ICI Business Link Partnership, the NASA Microgravity Program, and the State of Delaware.

References

1. P. Erhard and S. H. Davis, Nonisothermal spreading of liquid drops on horizontal plates. *J. Fluid Mech.* 229 (1991) 365–388.
2. L. D. Landau and E. M. Lifshitz, *Fluid Mechanics*. Oxford: Pergamon Press (1959).
3. S. K. Wilson, The effect of an axial temperature gradient on the steady motion of a large droplet in a tube. *J. Eng. Math.* 29 (1995) 205–217.
4. M. K. Smith, Thermocapillary migration of a two-dimensional liquid droplet on a solid surface. *J. Fluid. Mech.* 294 (1995) 209–230.
5. A. Mazouchi and G. M. Homsy, Thermocapillary migration of long bubbles in cylindrical capillary tubes. *Phys. Fluids* 12 (2000) 542–549.
6. T. S. Sammarco and M. A. Burns, Thermocapillary pumping of discrete drops in microfabricated analysis devices. *AIChE J.* 45 (1999)350–366.
7. V. Ludviksson and E. N. Lightfoot, The dynamics of thin liquid films in the presence of surface-tension gradients. *AIChE J.* 17 (1971 1166–1173.
8. A. M. Cazabat, F. Heslot, S. M. Troian and P. Carles, Fingering instability of thin spreading films driven by temperature gradients. *Nature* 346 (1990) 824–826.

9. A. M. Cazabat, F. Heslot, P. Carles and S. M. Troian, Hydrodynamic fingering instability of driven wetting films. *Adv. Coll. Interf. Sci.* 39 (1992) 61–75.
10. X. Fanton, A. M. Cazabat and D. Quere, Thickness and shape of films driven by Marangoni flow. *Langmuir* 12 (1996) 5875–5880.
11. V. G. Levich, *Physiochemical Hydrodynamics*. Englewood Cliffs: Prentice-Hall (1962) 700 pp.
12. S. D. R. Wilson, The drag-out problem in film coating theory. *J. Eng. Math.* 16 (1982) 209–221.
13. D. E. Kataoka and S. M. Trojan, A theoretical study of instabilities at the advancing front of thermally driven coating films. *J. Colloid Interf. Sci.* 192 (1997) 350–362.
14. D. E. Kataoka and S. M. Troian, Stabilizing the advancing front of thermall driven climbing films. *J. Colloid Interf. Sci.* 203 (1998) 335–344.
15. M. H. Eres, L. W. Schwartz and R. V. Roy, Fingering phenomena for driven coating films. *Phys. Fluids* 12 (2000) 1278–1295.
16. P. Carles and A. M. Cazabat, The thickness of surface-tension-gradient-driven spreading films. *J. Colloid Interf. Sci.* 157 (1993) 196–201.
17. H. Gau, S. Herminghaus, P. Lenz and R. Lipowsky, Liquid morphologies on structured surfaces; from microchannels to microchips. *Science* 283 (1999) 46–48.
18. N. V. Churaev and V. D. Sobolev, Prediction of contact angles on the basis of the Frumkin-Derjaguin approach. *Adv. Colloid Interf. Science* 61 (1995) 1–16.
19. B. V. Derjaguin, The definition and magnitude of disjoining pressure and its role in the statics and dynamics of thin fluid films. *Kolloid Zhurnal* 17 (1955) 205–214.
20. G. F. Teletzke, H. T. Davis and L. E. Scriven, Wetting hydrodynamics. *Revue de Physique Appliquee* 23 (1988) 989–1007.
21. V. S. Mitlin and N. V. Petviashvili, Nonlinear dynamics of dewetting: Kinetically stable structures. *Phys. Lett. A* 192 (1994) 323–326.
22. L. W. Schwartz, Hysteretic effects in droplet motions on heterogeneous substrates: Direct numerical simulation. *Langmuir* 14 (1998) 3440–3453.
23. L. W. Schwartz and R. R Eley, Simulation of droplet motion on low-energy and heterogeneous surfaces. *J. Colloid Interf. Sci*. 202 (1998) 173–188.
24. A. L. Bertozzi, A. Munch, X. Fanton and A. M. Cazabat, Contact line stability and undercompressive shocks in driven thin film flow. *Phys. Rev. Lett.* 81 (1998) 5169–5172.
25. A. L. Bertozzi, A. Munch and M. Shearer, Undercompressive shocks in thin film flows. *Physica D* 134 (1999) 431–464.
26. A. Munch and A. L. Bertozzi, Rarefaction-undercompressive fronts in driven films. *Phys. Fluids* 11 (1999) 2812–2814.
27. R. W. Atherton and G. M. Homsy, On the derivation of evolution equations for interfacial waves. *Chem. Eng. Comm.* 2 (1976) 57–77.
28. E. O. Tuck and L. W. Schwartz, A numerical and asymptotic study of some third- order ordinary differential equations relevant to draining and coating flows. *S.I.A.M. Rev.* 32 (1990) 453–469.
29. M. D. Van Dyke, *Perturbation Methods in Fluid Mechanics*. Annotated Edition. Stanford: Parabolic Press (1975) 271 pp.
30. H. M. Princen, The equilibrium shapes of interfaces, drops and bubbles. *Surf. Colloid Sci.* 11 (1969) 1–84.
31. C. Huh and L. E. Scriven, Hydrodynamic model of steady movement of a solid liquid fluid contact line. *J. Colloid Interf. Sci*. 35 (1971) 85–101.
32. J. A. Moriarty and L. W. Schwartz, Effective slip in numerical calculations of moving-contact-line problems. *J. Eng. Math.* 26 (1992) 81–86.
33. J. N. Israelachvili, Ĩntermolecular and Surface Forces, 2nd Ed. London: Academic Press (1992) 450 pp.
34. J. A. Moriarty and L. W. Schwartz, Dynamic considerations in the closing and opening of holes in thin liquid films. *J. Colloid Interf. Sci.* 161 (1993) 335–342.
35. D. E. Weidner, L. W. Schwartz and R. R. Eley, Role of surface tension gradients in correcting coating defects in corners. *J. Colloid Interf. Sci*. 179 (1996) 66–75.